

The Local Interstellar Medium in Puppis-Vela¹

Alexandra N. Cha², M. S. Sahu^{3,4}, H. Warren Moos², & A. Blaauw⁵

ABSTRACT

The first study of the local interstellar medium (LISM) toward Puppis-Vela ($l = 245^\circ$ to 275° , $b = -15^\circ$ to $+5^\circ$, $d < 200$ pc) is presented in this paper. A study of the locations, sizes, and physical characteristics of local interstellar gas, i.e. “astronephography,” is included, and relies upon the improved distance measurements provided by Hipparcos parallax measurements. All spectra of more distant sight lines contain absorption features due to intervening local gas, and more distant structures can only be studied accurately if components due to the LISM have been isolated. Towards this end, high resolution ($R \approx 95,000$), high signal-to-noise ($S/N \sim 110$ to 250) Na I $\lambda\lambda 5889.951$, 5895.924 spectra of 11 nearby stars in the direction of Puppis-Vela have been obtained with the Coudé Echelle Spectrograph on the 1.4 meter Coudé Auxiliary Telescope at the European Southern Observatory. Toward Puppis-Vela, absorption due to the Local Interstellar Cloud (LIC) was not observed, but components at three distinct velocities were found, and the extent of the local gas producing the features was estimated. The three components have the following locations and velocities: Component A—[$l \approx 276^\circ$ to 298° , $b \approx -5^\circ$ to $+4^\circ$], $V_{helio} = +6$ to $+9$ km s^{-1} , and $d \sim 104$ pc; Component B—[$l \approx 264^\circ$ to 276° , $b \approx -7^\circ$ to $+3^\circ$], $V_{helio} = +12$ to $+15$ km s^{-1} , and $d \sim 115$ pc; Component C—[$l \approx 252^\circ$ to 271° , $b \approx -8^\circ$ to -6°], $V_{helio} = +21$ to $+23$ km s^{-1} , and $d \sim 131$ pc. The conclusions regarding the ultraviolet spectrum of γ^2 Vel ($l = 263^\circ$, $b = -8^\circ$, $d = 258 \pm 35$ pc) presented by Fitzpatrick & Spitzer (1994) were re-examined in light of this new LISM data, and the ambiguity in their conclusions about several absorption components is resolved. The stars in Puppis-Vela flank the region of the apparent extension of the Local Bubble (or Cavity) known as the β CMa tunnel, and measurements of the Na I column density towards the sample stars have been used to modify existing estimates of the extent of the tunnel. A compilation of all existing Na I observations of < 200 pc sight lines around the tunnel reveal that low column densities have been exclusively detected within $l \approx 210^\circ$ to 250° , and $b \approx -21^\circ$ to -9° . Near the Galactic plane, at latitudes $-10^\circ < b < 0^\circ$ and $d \lesssim 150$ pc, the tunnel is confined to $l < 270^\circ$, a lower longitude than was previously reported.

¹Based on observations collected at the European Southern Observatory at La Silla, Chile

²Department of Physics & Astronomy, The Johns Hopkins University, Baltimore, MD 21218

³NASA/Goddard Space Flight Center, Code 681, Greenbelt, MD 20771

⁴National Optical Astronomy Observatories, 950 North Cherry Avenue, Tucson, AZ 87519-4933

⁵Kapteyn Instituut, Postbus 800, 9700 AV Groningen, The Netherlands

Subject headings: ISM: kinematics & dynamics — ISM: structure — Galaxy: solar neighborhood

1. Introduction

We view the Universe through local interstellar gas and this gaseous material in the immediate vicinity of the Sun affects all absorption line studies of more distant Galactic lines of sight.

The Local Interstellar Medium (LISM) in the direction of Puppis-Vela [$l = 250^\circ$ to 275° , $b = -15^\circ$ to $+5^\circ$] was selected for a Na I absorption line study to determine the kinematics of large-scale structures in the interstellar medium (ISM) toward Puppis-Vela, and was initiated by Sahu & Blaauw (1994). Within ~ 2 kpc in this direction, three large structures have been identified (1) the Vela Molecular Ridge at ~ 1 kpc (Murphy & May 1991), (2) the IRAS Vela Shell at ~ 450 pc (Sahu, 1992) and (3) the 36° -diameter, H α emitting Gum Nebula. Na I absorption caused by local ($d < 200$ pc) interstellar gas is present in spectra toward the distant background stars embedded in and beyond these extended objects. The absorption components arising within 200 pc must first be identified and understood before attempting to study the kinematics of more distant ISM structures. This work is the first attempt to three dimensionally (l,b,d) place components of interstellar gas in a localized region on the sky using optical absorption spectroscopy, and is preliminary to mapping clouds and extended structures at larger distances. The only interstellar clouds that have been mapped three dimensionally are the Local Interstellar Cloud (LIC) and G-cloud (Linsky *et al.* 2000) using principally H column densities from Hubble Space Telescope (HST) Space Telescope Imaging Spectrograph (STIS) and Goddard High Resolution Spectrograph (GHRS) spectra and the assumption that the clouds have constant density. For the Puppis-Vela sightlines discussed here, the technique of Linsky *et al.* cannot be applied since the Sun is not embedded in the gas under study and there is no evidence to allow the assumption that the lines of sight have constant density. Distances to target stars derived from Hipparcos parallax measurements allow limits to be placed on the extent of interstellar gas components, the first step in mapping the interstellar clouds or understanding the “astronephography” (Linsky *et al.* 2000) of the region. With multiple sight lines at various distances, recurring velocity features may be identified and used as a basis for defining the locations, sizes, and characteristics of interstellar gas.

Little is known about the LISM in Puppis-Vela within ~ 200 pc. In total, absorption line spectra of only five Puppis-Vela lines of sight have been published (Crawford 1991; Dunkin & Crawford 1999; Ferlet *et al.* 1985 and Welsh *et al.* 1994). There has been no localized, systematic study of the local gas toward Puppis-Vela until now. One implication of this lack of information is that LISM data must be obtained from all sky surveys (Welsh *et al.* 1998, Génova *et al.* 1997) whose velocity and column density generalizations may not be indicative of the nature of LISM gas in a specific direction. The identification of local velocity components toward Puppis-Vela performed here will allow local absorption features to be distinguished from more distant absorption features in any subsequent study of the ISM in Puppis-Vela. Questions posed by Puppis-Vela ISM

studies that are addressed here include: What is the contribution of the LIC in this direction? Does the Local Bubble (or Cavity) extend beyond ~ 70 pc in this direction? Are there any neutral velocity components in the LISM in Puppis-Vela?

We investigate the kinematics and structure of the LISM gas in Puppis-Vela using Na I absorption line data of 11 stars with Hipparcos-based distances < 200 pc, in conjunction with data for five previously studied lines of sight. The Na I spectra presented here form a subset of a larger sample containing absorption spectra toward ~ 75 more distant stars in Puppis-Vela, which corroborate the conclusions made here, and will be presented in a subsequent paper.

2. Components of the LISM

It is helpful to review the structures contained in the LISM to more fully understand the Puppis-Vela lines of sight. The three known components of the LISM include the Local Interstellar Cloud (LIC), the G cloud, and the Local Bubble. The Sun is moving through a warm ($T \sim 7000$ K), low density ($n(\text{H I}) \sim 0.1 \text{ cm}^{-3}$), partially ionized interstellar cloud termed the LIC (Lallement & Ferlet 1997, Lallement & Bertin 1992). Figure 1 shows a schematic diagram of the components of the LISM as viewed from above the plane of the Galaxy. The LIC is observed in projection toward most but not all nearby stars, and extends approximately 3 – 8 pc. The LIC is the only interstellar cloud where *in situ* measurements of interstellar dust grains (Baguhl *et al.* 1996) and interstellar gas (Witte *et al.* 1992) have been performed through *Ulysses* & *Galileo* spacecraft observations. Models of the LIC (Redfield & Linsky 1999) place the Sun just inside the LIC, in the direction of the Galactic Center and toward the North Galactic Pole. The Solar Wind is carving out a cavity in the LIC which is slightly elongated in the direction of relative motion of the Sun in the LIC. In the direction of the Galactic Center, another cloud termed the G cloud is seen. This cloud is colder ($T \sim 5400$ K) (Linsky & Wood 1996) and is approaching the Sun at about 29 km s^{-1} . From Figure 1, it is clear that the G cloud is not expected to be seen in the Puppis-Vela direction. Since the Sun is within the LIC, interstellar sight lines in all directions contain absorption from gas associated with the LIC, but these features are not always strong enough to be detected in Na I absorption. Specifically toward Puppis-Vela, very low Na I column densities of $\sim 10^8$ to 10^9 cm^{-2} can be estimated using the empirical $N(\text{H})/N(\text{Na I})$ formula given by Ferlet *et al.* (1985), and low color excesses, $E(\text{B} - \text{V}) \leq 0.06$, are detected toward $d < 200$ pc Puppis-Vela sight lines. Very low electron column densities ($n_e \lesssim 0.03$) are also deduced from the dispersion measure of three pulsars within 200 pc (Toscano *et al.* 1999).

Surrounding the Sun, the LIC, and the G cloud is the Local Bubble (or Cavity). The Local Bubble is an irregularly shaped region that radially extends approximately 70 pc from the Sun (Welsh *et al.* 1998). The Local Bubble appears to protrude toward β CMa [$l = 226^\circ$, $b = -14^\circ$], forming an extention called the β CMa tunnel and borders the sight lines to Puppis-Vela. The extent of the tunnel is not well determined, and is discussed in detail in §6.3. It is not yet known whether the Local Bubble is a bounded region created from a cataclysmic event such as a supernova

explosion, or if the Local Bubble is an intercloud region, isolated by the boundaries of neighboring structures (Snowden *et al.* 1990). The majority of the volume of the Local Bubble is filled with hot X-ray emitting plasma with a characteristic temperature of $T \sim 10^6$ K, while most of the mass in the Local Bubble is cool and diffuse ($T \sim 100$ K). Typical densities in the Local Bubble range between $\sim 0.002 - 500$ cm $^{-3}$ (for a recent review on this subject see Breitschwerdt (1998)).

3. Using Na I to study the LISM

There are advantages and disadvantages associated with using Na I to study the LISM. The main advantage of Na I is that it is possible to perform high resolution ($R \sim 100,000$) surveys with ground based telescopes. Na I is a tracer of cold, high column density gas since it has a low ionization potential of 5.14 eV. On the other hand, the disadvantage of observing Na I is that it is a trace ion in the ISM. Na I is well suited for mapping the boundaries of hot plasma in the Local Bubble since low column densities of Na I are expected within the Local Bubble and higher column densities are detected without. Additionally, cold clouds are embedded in the hot Local Bubble, and these clouds may be located and mapped with Na I. Estimates on the extent, distance, velocity and Na I column density of previously undocumented components containing neutral gas are presented in §6.

The most abundant species in the LISM is H I; however, H I is more difficult to observe since space based instruments must be employed to measure its column density. There are two empirical methods by which column densities of H I may be estimated: the ratio of $N(H\,I):E(B-V)$ (Bohlin *et al.* 1978, Diplas & Savage 1994), and the ratio of $N(H):N(Na\,I)$ (Hobbs 1974a, 1974b, 1976, Stokes 1978, and Ferlet *et al.* 1985). Neither of these two methods of empirically calculating $N(H\,I)$ are suitable for the study of the LISM toward Puppis-Vela.

The first method of calculating atomic hydrogen column densities given the color excesses of stars does not produce accurate results for sight lines with very low reddening since the uncertainties associated with the MK spectral type are large compared to the observed values of $(B-V)$. The second method of determining the distribution of hydrogen estimates $N(H\,I + H_2)$ given column densities of Na I is also inaccurate for regions of low column density. The studies mentioned above contain few data points for $N(Na\,I) \lesssim 10^{11}$ cm $^{-2}$. Nearly 80% of the local Puppis-Vela LISM sight lines contain absorption components with column densities below 10^{11} cm $^{-2}$, the regime where the $N(H)$ to $N(Na\,I)$ empirical relationship has not been shown to apply. In addition to the lack of data points in the low column density limit, Welty *et al.* (1994) have also noted that several of the low column density data points are incorrect. The large uncertainty in $N(H):N(Na\,I)$ in the low column density limit makes it useful for only order of magnitude estimates. As a point of reference, however, direct H I observations along several lines of sight in Puppis-Vela at $d \sim 100$ pc exhibit $\log N(H\,I) \approx 18.1$ to 20.1 cm $^{-2}$ (Table 5.1, Dring 1997).

4. Observations and Data Reduction

Na D₁ and D₂ $\lambda\lambda 5889.951, 5895.924$ spectra for 11 B-type stars within 200 pc in the direction of the IRAS Vela Shell (l, b) $\approx (263^\circ, 8^\circ)$ were obtained by M. S. Sahu and A. Blaauw using the Coudé Echelle Spectrograph (CES) on the 1.4 meter Coudé Auxiliary Telescope (CAT) at the European Southern Observatory. The observations were made both on site in La Silla and remotely from Garching in January 1993 (HD 76805) and January 1994. The Long Camera and the UV-coated Ford Aerospace/Loral 2048 \times 2048 CCD (#27) were used for all observations. The CCD's pixel size was $15 \mu\text{m} \times 15 \mu\text{m}$, and had a low dark current of $3 \text{ e}^-/\text{pixel}/\text{hour}$, a low readout noise ($\sim 6\text{e}^- \text{ rms}$), and few apparent defects. The net efficiency of the system is 3.8% at 5400 Å and 4.6% at 6450 Å (Pasquini *et al.* 1992).

Table 1 contains general stellar information for the 11 stars observed. To supplement the sample, we searched the literature and found five additional stars with Na I column density and velocity measurements in the direction towards Puppis-Vela. The following information is listed for each star: HD number, Galactic position (longitude and latitude), MK spectral type classification, visual magnitude, observed Johnson photometric colors from the Tycho catalogue, calculated B–V color excess, distance obtained using Hipparcos trigonometric parallax data, heliocentric radial velocity (V_{rad}), projected rotational velocities ($v \sin i$), and references for the MK spectral type and V_{rad} , respectively.

A standard data reduction procedure was followed that first included bias subtraction and flat-fielding of the science spectra. A thorium-argon arc lamp was the wavelength calibration source, and the stability of the CES yielded unchanging calibration exposures throughout each night. The calibration spectra were used in conjunction with the Th-Ar line list by Willmarth (1987) to visually identify the emission lines, fit a second degree polynomial to the resulting pixel vs. wavelength arrays, and thereby convert our absorption line spectra from pixel to wavelength space. The absolute wavelength solutions had rms variations of 0.7 km s^{-1} or 0.014 \AA for the 1993 spectrum and 1.1 km s^{-1} or 0.023 \AA for the 1994 spectra. The instrumental resolution determined using the FWHM of the thorium lines for both observing runs was 3.1 km s^{-1} , equivalent to $\lambda/\Delta\lambda \approx 95,000$.

In addition to the interstellar Na I absorption features, the raw spectra were contaminated by many telluric absorption lines which are abundant at wavelengths surrounding the Na I D doublet. Multiple observations of α Vir (HD 116658) were made since it is a nearby star with a high rotational velocity ($v \sin i = 159 \text{ km s}^{-1}$, Hoffleit & Jaschek 1982) and little interstellar Na I absorption. These spectra were used as templates to remove telluric absorption lines contaminating the spectra. To normalize the template spectra, the continua were fit with cubic splines then divided by the fits. The optical depths of the atmospheric absorption lines in α Vir were adjusted by a multiplicative factor for each star so that the strength of the well separated telluric lines at wavelengths of 5883–5901 Å matched those in each object spectrum. Next, the object spectra were divided by the scaled α Vir template spectra to eliminate telluric absorption lines. The observed

spectra were continuum normalized by fitting a cubic spline and dividing the object spectrum by the fit. The resulting spectra had signal-to-noise ratios of 110 to 250.

5. Presentation of the Data

To fit the spectral lines and infer physical properties about the interstellar velocity components along each line of sight, we used the profile fitting method and software developed by Welty, Hobbs, & Kulkarni (1994). This technique assumes that the components have Maxwellian velocity distributions. Each line was fit with the fewest number of components necessary, and additional components either increased the χ^2 statistic or required that one or more components have unphysical b values. The parameters describing each component were adjusted by an iterative, non-linear, least-square method to achieve an rms deviation of the absorption line fit that was comparable to the rms deviation in the stellar continuum, and reduced the value of the χ^2 statistic.

The Na I spectra of the 11 stars observed are displayed in Figure 2. For each sight line, normalized intensity is plotted versus heliocentric velocity for both the D_2 and D_1 lines. Filled circles indicate the data points, the best-fit models are plotted with solid lines, and dashed lines trace the individual Gaussian components. Beneath the D_1 spectra are the residuals to the fits for the D_2 lines. For the spectra of HD 72232 and HD 79416, the y-axes in the residual plots range from -0.1 to 0.1 in units of normalized intensity, whereas for the rest of the spectra, the y-axes of the residual plots range from -0.015 to 0.015 . Upwards arrows beneath the D_2 lines are located at the projected LIC velocity. No LIC components are revealed in the spectra, as expected (see §2).

Table 2 contains numerical data associated with the model fits and includes: (1) the HD number, (2) central heliocentric velocity, (3) equivalent width, (4) Doppler b parameter, (5) logarithm of the Na I column density, (6) signal-to-noise ratio, and (7) the heliocentric to LSR velocity conversion factor. Uncertainties were estimated by comparing the measured Na I D_2 and D_1 profile fit parameters. If there were no sources of error, these values would be identical since each pair of doublet lines arise due to absorption by the same Na I gas. The maximum difference in measured velocities between a D_2 versus D_1 component is $\pm 0.5 \text{ km s}^{-1}$, and is consistent with the calculated rms velocity dispersion. The uncertainties associated with the column density and b value are generally $< 10\%$ and a quality estimate is listed for each spectral line in Table 2.

6. Discussion

6.1. Identification of Three Velocity Components

Along the eleven sight lines toward early type stars located within $250^\circ < l < 299^\circ$ and $-8^\circ < b < +4^\circ$, Na I gas is primarily found in one of three distinct velocity ranges (to an accuracy of $\sim 1 \text{ km s}^{-1}$) . Five additional sight lines with Na I kinematic information were found in the

literature. General stellar information for these stars is listed in Table 3. Information about the Na I components observed is in Table 4 and includes: (1) HD number, (2) central heliocentric velocity, (3) Doppler b parameter, (4) logarithm of the Na I column density, (5) velocity resolution at which the observation was made, and (6) a reference for the data.

Although the sixteen lines of sight are spread over $\sim 50^\circ$ in Galactic longitude, the absorption components do not appear at random velocities. The majority of the velocity components can be associated with one of the following velocity ranges: (A) $+6 \text{ km s}^{-1} < V_{helio} < +9 \text{ km s}^{-1}$, (B) $+12 \text{ km s}^{-1} < V_{helio} < +15 \text{ km s}^{-1}$, and (C) $+21 \text{ km s}^{-1} < V_{helio} < 23 \text{ km s}^{-1}$. The Galactic coordinates of the sixteen lines of sight have been plotted in Figure 3. Filled triangles indicate the locations of stars whose we present new Na I data, while open triangles pinpoint the locations of stars for which data are from the literature. To illustrate the presence of absorption components at the three common velocities described, lines of sight with absorption at velocities A, B, and C have been encircled. No distinction has been made regarding the source of the data in Figures 3b-3d. The symbol sizes indicate the relative Na I column density detected. Small symbols correspond to $10.0 < \log[N(\text{Na I})] < 10.4$, medium symbols denote $10.4 < \log[N(\text{Na I})] < 11.1$, and large symbols represent column densities of $11.7 < \log[N(\text{Na I})] < 12.6$.

Analysis of the distribution of data points in Figure 3 reveals that velocity components A, B, and C are located at distinct regions in l and b . The size of the data points, which corresponds to the Na I column density, reveals that higher column densities of gas at velocities A and B exist in this region of the LISIM, whereas the sight lines with absorption at velocity C have lower column densities. Comparing the locations where each of the components are detected, the velocities of the components in the Local Standard of Rest decrease with increasing Galactic longitude. General Galactic rotation also follows this trend, but the Galactic rotation velocities calculated at $d = 150 \text{ pc}$, assuming a galactocentric distance of 8.5 kpc, and a local circular speed of 220 km s^{-1} in the solar neighborhood (Mihalas & Binney 1981), do not match up with the velocities of Na I absorption features observed in the LISIM. The sightlines to stars at $d > 200 \text{ pc}$ confirm the locations of local gas absorption for components B and C, whereas the region $280^\circ < l < 300^\circ$, where component A is detected, is outside of the sample area. Also from the spectra of the more distant sight lines, absorption features at the velocity of Component B were additionally observed along sightlines with $b \gtrsim -10^\circ$ and $l \gtrsim 260^\circ$, and gas with velocities coincident with Component C was observed up to the Galactic plane ($b \lesssim 0^\circ$).

In Figure 4 the Puppis-Vela region is viewed from above the Galactic plane and contains the same data points as Figure 3. Here, distance increases radially outward and galactic longitude increases counterclockwise. The symbol sizes are defined identically as in Figure 3, and the same Galactic latitude range is applied: $-10^\circ < b < +5^\circ$. The symbols in Figure 4 indicate the velocity of the absorption component, and have been placed at the appropriate distance and galactic longitude of the target star. From this perspective, the locations of components with similar velocities are also seen to be grouped together, and not randomly distributed. Arcs have been overplotted to highlight the maximum distance and minimum extent in Galactic longitude of the front edge of

a gas component at a particular velocity. The arcs have been labeled with “A,” “B,” or “C” to match the velocity ranges defined above and on the plot. Note that the arc labeled “C” is dashed in the center to indicate where its presence is uncertain according to the spectra presented here, but when spectra from more distant stars are included, gas with velocity C is seen throughout the entire Galactic longitude range.

The locations and characteristics of the three components are summarized in Table 5. For each component, Table 5 lists the minimum extent in Galactic longitude and latitude where the gas is observed, the maximum distance to the gas, the heliocentric velocity range of the gas, and the spread in Na I column densities for spectral lines within the given velocity range. Three stars (HD 61831, HD 65575, and HD 74195) have been omitted from Figure 4 for reasons discussed in §6.3.

Sight lines either pass completely through the component, or partially penetrate the gas. Using the distribution of the measured column densities towards the target stars of known distances, it is possible to deduce limits on the distances to each gas component. Refining these distance estimates would necessarily require more observations (~ 18 additional sight lines exist) to obtain a finer distribution of observations so that the boundaries of the gas and the density distribution of the gas within the components could be distinguished. Specific characteristics of the gas at velocities A, B, and C are suggested below.

The three components of gas observed in the LISM have unique characteristics. Sight lines with velocity A gas exhibit rather high column densities (large symbols) along three out of four sight lines. These three high column density sight lines (#1, 3, 8) are located at Galactic latitudes of $-4.9^\circ < b < -3.0^\circ$, while the fourth target whose spectrum exhibits gas with velocity A is at $b = +3.8^\circ$. Since the latitude of the latter target, HD 106490, is on average 8° away from the others, a smaller column density of gas at $V_{helio} = +6$ to $+9 \text{ km s}^{-1}$ exists above the galactic plane towards HD 106490 (#2). The absorbing material is confined to a distance $< 100 \text{ pc}$ since the column density of Na I does not increase when more distant sight lines are observed.

Sight lines with components at velocity B tend to have moderate to high column densities at larger distances. Toward the stars HD 79416 (#9) and HD 72232 (#10) we find $\log N(\text{Na I}) \sim 11.8$, whereas the remainder of the sight lines with absorption at velocity B ranged from $\log N(\text{Na I}) = 10.28$ to 11.08 . Towards one of the seven stars with spectral features at velocity B, HD 74560 has a low column density (small symbol), yet it is physically located between several stars that have substantially higher column densities. This variation in the magnitude of the column densities suggests that the velocity B gas is patchy, and inhomogeneous. The high column density along the line of sight towards HD 74195 (#8), observed by Welsh *et al.* (1994), reveals gas at velocity B, however the Doppler parameter given, $b = 0.3 \pm 0.1 \text{ km s}^{-1}$ is small compared to the 3.6 km s^{-1} velocity resolution, so this data point has been omitted from our analysis.

There are two concentrations of sight lines with velocity C gas: one at $l \approx 270^\circ$ and one at $l \approx 252^\circ$. Low column densities (small symbols) are observed towards the stars grouped at $l \approx$

270° while moderate column densities (medium symbols) are seen toward $l \approx 252^\circ$. Stars HD 74146 (#5), HD 74071 (#6), and HD 74560 (#7) may be located near the edge of the component or the component may be very diffuse considering the low values of N(Na I) detected.

Because of the absence of observed sight lines with $d < 200$ pc, the arc tracing the estimated boundary of velocity C gas is dashed in the middle. Three nearby stars are located behind the dashed portion of the arc but do not exhibit absorption by gas at velocity C in their Na I spectra. As noted above, it is likely that the gas is patchy and inhomogeneous, which would then account for the observations. The presence of component C in the spectra of the longer sight lines in the sample is also intermittent, also indicating that the component C gas is patchy. One of these stars, HD 79416 (#10), is located above the Galactic plane at $b = +3.3^\circ$, while all of the stars revealing velocity C gas have $b \leq -5.9^\circ$. The spectra from the more distant stars in our sample include component C gas for $b \lesssim 0^\circ$ and for the same extent in l .

With the components of neutral Na I gas arising in the first 200 pc of the ISM toward Puppis-Vela identified, any subsequent spectroscopic study of the neutral ISM in this direction can distinguish between local gas and more distant gas. The presence of absorption components at velocities A, B, or C in the spectra of future studies will not be confused with absorption due to the myriad other structures that exist toward Puppis-Vela. The three dimensional information about the components—the extent of the gas as projected on the sky, and the limits on the distance to the gas—serve as a basis of estimating the typical velocities and column densities present in the LISM.

In general, the LISM toward Puppis-Vela has low positive velocities ranging from $+6 \text{ km s}^{-1}$ to $+23 \text{ km s}^{-1}$. Absorbing gas at these velocities is located at distances closer than ~ 104 pc, and the Na I column densities detected range from $\log N = 10.2 \text{ cm}^{-2}$ to 11.9 cm^{-2} indicating that the cold gas is clumpy or patchy, and not uniformly distributed.

6.2. Using LISM Component Data—An Example

To put our results in perspective, we searched the literature for UV interstellar absorption line studies in the direction of Puppis-Vela in order to demonstrate that knowing the properties of the LISM gas in a particular region of the sky is extremely valuable for the interpretation of longer lines of sight. The only recent study has been toward γ^2 Velorum by Fitzpatrick & Spitzer (1994; hereafter FS94). Their *Hubble Space Telescope (HST)*/Goddard High-Resolution Spectrograph (GHRS) observations have a velocity resolution similar to our Na I data (3.1 km s^{-1} versus 3.5 km s^{-1} for the GHRS data) facilitating a comparison between the two datasets. γ^2 Velorum is located at $[(l = 263^\circ, b = -8^\circ); d \approx 260 \text{ pc}]$ so it is likely that some of the components observed in the GHRS spectra arise in the LISM. FS94 detect seven components as described in Table 6. Comparing the velocities of the FS94 features with the three velocity components we detect in the LISM, their component 6 corresponds to our component C and their components 4 and 5 correspond to our component B.

The neutral species detected with GHRS include S I and C I. FS94 fit the S I spectrum with component 4, and the C I feature with components 2 and 4. In addition to these neutral species, we also include a Na I spectrum of γ^2 Vel that was obtained at the same time and with the same instruments as the LISM data toward Puppis-Vela described in §4. The Na I D₂ and D₁ spectra of γ^2 Vel are shown in Figure 5, and the parameters of the fit are listed in Table 7. Na I absorption is seen at velocities corresponding to FS94 components 2, 4, and 6. Comparing the Na I data for the γ^2 Vel line of sight with the distribution of gas in the foreground, we may conclude that component 2 arises in gas located beyond 200 pc, yet less than 260 pc—the distance to γ^2 Vel. Both components 4 and 6 were detected in the LISM at distances < 200 pc.

The presence of component 4 is complicated, however, by the fact that it appears in the spectra of all of the species detected in FS94, both neutral and highly ionized, and in our Na I spectrum. In addition, FS94 note that a *Copernicus* spectrum toward γ^2 Vel reveals H₂ absorption which may be assigned to either component 4 or a blend of components 2 and 5. Although FS94 assign H II region origins to component 4 absorption because of the presence of species such as C IV and Si IV, it is difficult to reconcile neutrals and molecules coexisting with such highly ionized species.

FS94 propose that the H II region containing the component 4 gas is the ~ 40 pc surrounding a ~ 60 pc-radius stellar wind blown bubble centered on γ^2 Vel. We suggest that there are two distinct regions of gas with velocities matching component 4. First, the ionized region extending 100 pc from the star described in FS94 contains ionized gas at $V_{helio} \approx 13 \text{ km s}^{-1}$. Second, the neutral gas absorption along the line of sight to γ^2 Vel at $V_{helio} \approx 13 \text{ km s}^{-1}$ occurs at $d \approx 115$ pc, corresponding with our component B. If the H₂ spectrum is fit by component 4, then it is consistent to place the H₂ gas with the Na I in component B, thereby providing a unique example of H₂ gas near the edge, or possibly within, the Local Bubble.

Not only is the mapping of the nearby gas essential in the characterization of the LISM itself, this data clarified the complex absorption signature along the γ^2 Vel line of sight, and should prove useful for other Puppis-Vela sight lines. Caution must be observed, however, since it has been shown here and in other papers (Watson & Meyer (1996); Frail *et al.* (1994); Lauroesch *et al.* (1998, 1999)) that interstellar Na I is patchy, as evidenced by the subparsec-scale structures that appear to be ubiquitous in the diffuse ISM, but this focused study will detect most components specific to the Puppis-Vela LISM which previous all-sky local gas surveys ignored.

6.3. LISM Absorption Components at Peculiar Velocities

Of the 27 absorption features detected (excluding the ultra-high resolution data of Dunkin & Crawford (1999)) along 16 lines of sight, 9 features have velocities outside of velocities A, B, and C. The peculiar velocities of all but three components can be understood with simple explanations. A total of three absorption components toward HD 61831 and HD 72232 lie just outside of the velocity ranges A, B, and C. It is likely that these absorption features are blends of multiple narrow lines

that are unresolved at $R \sim 100,000$, as evidenced by the many components distinguished in the ultra-high resolution data towards HD 81188 cited in Table 4. Three additional components toward HD 65575 and HD 106490 have peculiar velocities, but these stars are located at the periphery of the sample, and it is natural that at some point the characteristics of the gas change and components A, B, and C cease being detected.

In total, only 3 of 27 components cannot be simply accounted for, and they include the $V_{helio} = +132.3 \text{ km s}^{-1}$ and -10.6 km s^{-1} lines toward HD 62226 and the $V_{helio} = -139 \text{ km s}^{-1}$ line toward HD 74146. The spectra of HD 62226 and HD 74146 are plotted in Figure 6a and 5b, respectively. For each line of sight, the Na I D₂ absorption is plotted at the top, the D₁ absorption is plotted in the middle of the panel. The residual to the best fit to the D₂ spectrum is on the bottom, plotted with the y-axis ranging from -0.015 to $+0.015$. Unlike the spectra of the other LISM sight lines in this region, that of HD 62226 contains three components at three distinct velocities. The absorption at $V_{helio} = +22.2 \text{ km s}^{-1}$ is consistent with the gas observed towards adjacent sight lines in the region, but the absorption features at $V_{helio} = -10.6 \text{ km s}^{-1}$ and $+132.2 \text{ km s}^{-1}$ are not observed towards any other stars in the area.

Although lines of sight adjacent to HD 62226 were also observed, namely HD 61878, HD 64503, and HD 61831, the spectra toward these stars do not show absorption at either $V_{helio} = -10.6 \text{ km s}^{-1}$ or $+132.2 \text{ km s}^{-1}$. Because the sight line towards HD 62226 is fortuitously flanked by these three nearby lines of sight that have also been observed, it may be concluded that the gas producing the $V_{helio} = -10.6 \text{ km s}^{-1}$ and $+132.2 \text{ km s}^{-1}$ components are confined to a small region projected on the sky at $d < 190 \text{ pc}$. The $V_{helio} = -10.6 \text{ km s}^{-1}$ component is very weak, but is clearly visible in both the D₂ and D₁ spectra. The D₂/D₁ ratio of equivalent widths for the $+132.2 \text{ km s}^{-1}$ lines equals 2.2, which is close to the expected ratio of 2 for unsaturated Na I D₂ and D₁ lines.

The other sight line with unexplained components is that of HD 74146 which also contains an absorption component at a high velocity, but here the feature is a broad ($b = 16.7 \text{ km s}^{-1}$) line at negative velocity, $V_{helio} = -139 \text{ km s}^{-1}$, and $D_2/D_1 = 0.8$. The breadth of the line and the low D₂/D₁ ratio are atypical of unsaturated interstellar lines, and it is unlikely that such a weak line could be saturated. Additionally, several sight lines adjacent to HD 74146 were also observed (HD 76805, HD 74071, and HD 74560) though their spectra did not reveal absorption at high negative velocities.

A literature search for information regarding whether or not circumstellar material has been observed around HD 62226 or HD 74146 yielded nothing. Additionally, we attempted to use *International Ultraviolet Explorer* (IUE) spectra to determine the origin of the high velocity absorption features. HD 74146 was not observed with IUE, and only one high dispersion spectrum of HD 62226 was obtained. The single spectrum toward HD 62226 had a low signal-to-noise ratio ($S/N < 10$), so the presence or absence of high velocity features associated with characteristic circumstellar or interstellar absorption could not be ascertained. With the data available, we were *not* able to determine whether the high velocity features in the spectra of HD 62226 and HD 74146 were of

circumstellar or interstellar origin.

6.4. The β CMa Tunnel

In §2 it was mentioned that the extension of the Local Bubble (or Cavity) known as the β CMa tunnel is adjacent to Puppis-Vela when projected on the sky. This tunnel of rarefied hot gas has been estimated to extend \sim 250-300 pc (Sfeir *et al.* 1999; Welsh 1991; Welsh, Crifo, & Lallement 1998), and appears to be almost free of neutral gas. For instance, H I column densities of $N(H I) \sim 10^{18} \text{ cm}^{-2}$ measured toward the 153 ± 15 pc line of sight to β CMa are thought to arise primarily in gas along the first \sim 5 pc—within the LIC (Gry *et al.* 1985). In this section, previous estimates of the tunnel’s extent will be reviewed and a new measurement of the size of the tunnel, within the first 150 pc, will be presented.

After the low gas densities towards several stars in the direction of β CMa were noticed, subsequent studies of the LISM probed adjacent sight lines to ascertain the size of the tunnel. Using optical absorption spectroscopy to observe the Na I D doublet, three estimates of the extent of the tunnel were made. First, Welsh (1991) assigned minimum angular dimensions to the tunnel: an elliptical hole located at $226^\circ \lesssim l \lesssim 242^\circ$, $-11^\circ \lesssim b \lesssim -20^\circ$, extending to a depth of \sim 300 pc. Later Welsh, Crifo, & Lallement (1998) revised the size of the tunnel and substantially widened the estimate. They reported minimum approximate dimensions of the low gas density tunnel towards β CMa to be 250 pc long by 90 pc wide. Analysis of Figure 2 in Welsh *et al.* indicates that the tunnel narrows at larger distances; specifically, the extent of the tunnel is $210^\circ \lesssim l \lesssim 277^\circ$ at $d = 150$ pc, while at $d = 250$ pc regions of higher column density gas bound the tunnel to within $215^\circ \lesssim l \lesssim 240^\circ$. Sfeir *et al.* (1999) included the β CMa tunnel in their maps of the neutral gas associated with the Local Bubble, but used only a few data points to confine the low gas density tunnel. Their data is inconclusive regarding the depth of the tunnel and they proposed that the tunnel is either terminated at a distance of \sim 250 pc by Na I absorbing gas producing equivalent widths of \sim 50 mÅ, or that the boundary of the tunnel is closer but contains several perforations.

The maps illustrating the tunnel in Welsh *et al.* (1998) and Sfeir *et al.* (1999) do not represent differences in the stars’ Galactic latitude, however. Both papers show the tunnel on plots of distance versus Galactic longitude with the stars projected onto the Galactic plane, thus obscuring information regarding the Galactic latitude of the target stars. Almost all of the published Na I spectral data in the direction of β CMa pertain to stars below the Galactic plane at $b \sim -10^\circ$ to -30° . Our observations add a new dimension to the tunnel boundary since the target stars in our sample are concentrated within $b \sim -10^\circ$ to 0° .

In addition to the Na I column density measurements given in Tables 2 and 4 for stars toward Puppis-Vela, $N(Na I)$ measurements along sight lines in and around the β CMa tunnel were compiled. Stellar information (as was given in Table 1) about these published sight lines is in Table 8, and the corresponding Na I column densities and references are in Table 9.

The column densities toward sight lines listed in Tables 2, 4, and 9 and projected onto the Galactic plane are illustrated as a function of distance and Galactic longitude, in Figure 7. The Galactic latitudes of the lines of sight have been divided into two groups: those at $-10^\circ < b < 0^\circ$ are indicated with filled symbols, while targets located at $-30^\circ < b < -10^\circ$ are plotted using open symbols. Diamonds are used when precise measurements of the Na I column density are known and triangles are plotted for sight lines where only $N(\text{Na I})$ upper limits have been determined. The symbol sizes suggest the relative column density detected along each line of sight, with larger symbols indicating larger column densities, as defined in the caption to Figure 3.

The thin solid lines in Figure 7 depict the longitudinal angular extent of the tunnel estimated by Welsh (1991). In view of the data shown in Figure 7, it appears that his estimate should be expanded by $\sim 5^\circ$ on either edge out to a distance of ≈ 150 pc. Note that all of the sight lines supporting this tunnel estimate have $b < -10^\circ$. So far, no observations have been made to constrain the tunnel’s extent in latitude or length. The expanded extent of the tunnel proposed by Welsh *et al.* (1998) (in their Figure 2) is sketched in Figure 6 with dotted lines. With the additional lines of sight near the Galactic plane presented here, the Welsh *et al.* high longitude tunnel boundary appears misplaced. Either one or more of the following reasons may account for this. The new data reveals that the first ~ 150 pc of the β CMa tunnel do not extend beyond $l \approx 267^\circ$, near the plane of the Galaxy ($-10^\circ < b < 0^\circ$). There is no data to confirm if the tunnel does or does not extend beyond $l = 267^\circ$ for $-30^\circ < b < -10^\circ$. At distances of ~ 150 to 200 pc, the tunnel does not extend beyond $l \approx 251^\circ$ near the plane of the Galaxy, as evidenced by the filled data points at $l > 250^\circ$ in Figure 7. There is no observational evidence to determine whether the β CMa tunnel extends past $l \approx 250^\circ$ at lower Galactic latitudes, since no sight lines have been observed there. The lower Galactic longitude boundary also appears to encompass sight lines with high Na I column densities, and should be relocated to $l \gtrsim 215^\circ$. From the compilation of data on almost 40 lines of sight, it appears that outside the Local Bubble ($d > 70$ pc), low neutral gas densities are to be found between $l \approx 215^\circ$ to 250° and $b \approx -21^\circ$ to -9° . The arc drawn in Figure 7 at $d \sim 150$ pc illustrates the extent in Galactic longitude over which low column density lines of sight with $b \lesssim -10^\circ$ have been observed. The arrows pointing to larger distances suggest that this bound on the β CMa tunnel is only a lower limit, but is dictated by the present data.

The most distant sight lines included in this sample have $d \sim 200$ pc and $b \sim -30^\circ$. At this limit, the sight lines have not penetrated the scale height of the disk of the Galaxy (see Dame & Thaddeus (1994) and Dickey & Lockman (1990)). Studies of more distant sight lines attempting to map the distant end of the tunnel could easily be confused by the Galactic disk’s decreasing density gradient, whereby stars at large distances and lower latitudes might exhibit lower $N(\text{Na I})$ measurements because of the geometry of the Galaxy, and not necessarily because of extensions in the Local Bubble. From nearby interstellar Na I measurements, there is a region of low density towards β CMa, but it is not clear whether the tunnel is present in the plane of the Galaxy. Additional observations along sight lines 0° to 30° below the Galactic plane are needed to clarify the three dimensional extent of the β CMa tunnel.

7. Conclusions

We have presented high resolution Na I spectra toward 11 early type stars plus kinematic data for 5 lines of sight taken from the literature to study the LISM in the direction of Puppis-Vela. Additionally, we have compiled a list of Na I column density measurements made toward nearby ($d < 200$ pc) sight lines in the β CMa tunnel. Our conclusions are stated below:

1. Observations of Na I in the LISM toward Puppis-Vela revealed absorption at three distinct velocities with the following properties: Component A—[$l \approx 276^\circ$ to 298° , $b \approx -5^\circ$ to $+4^\circ$], $V_{helio} = +6$ to $+9$ km s^{-1} , and $d \sim 104$ pc; Component B—[$l \approx 264^\circ$ to 276° , $b \approx -7^\circ$ to $+3^\circ$], $V_{helio} = +12$ to $+15$ km s^{-1} , and $d \sim 115$ pc; Component C—[$l \approx 252^\circ$ to 271° , $b \approx -8^\circ$ to -6°], $V_{helio} = +21$ to $+23$ km s^{-1} , and $d \sim 131$ pc. This identification of LISM gas will enable future studies of the Puppis-Vela ISM to separate local gas absorption from more distant features, as was illustrated for the γ^2 line of sight. Including a distinction of the distance at which gas exists, as well as its position on the sky, is a fundamental step in the new field of three dimensional astronephography.
2. The LIC is not detected in Na I absorption toward Puppis-Vela because the column densities of LIC gas in this direction are too low, generally $< 10^{11} \text{ cm}^{-2}$.
3. Low column density sight lines in the β CMa tunnel are confined to $l = 215^\circ$ to 250° and $b = -21^\circ$ to -9° , to a distance of ~ 150 pc. New observations closer to the Galactic plane ($-10^\circ < b < 0^\circ$) reveal higher column densities suggesting that the tunnel may not extend in latitude to $b = 0^\circ$. More observations near the Galactic plane and at distances greater than 150 pc are needed to ascertain the true size and location of the β CMa tunnel.
4. Although most of the absorption components seen in the spectra of stars within 200 pc toward Puppis-Vela could be assigned to one of the three components, A, B, or C, a few components had peculiar velocities. Toward HD 62226 and HD 74146 high velocity features, $V_{helio} = +132.2$ km s^{-1} and $V_{helio} = -139$ km s^{-1} respectively, were present. In both cases, nearby sight lines were also observed and contained no high velocity features. The origin of the high velocity gas components, be they circumstellar or interstellar, is unknown.

ANC and HWM acknowledge support from NASA contract NAS 5-32985 to Johns Hopkins University and MSS acknowledges support from a GTO grant to the STIS IDT. We thank F. Bruhweiler, W. Landsman, and J. Lauroesch for helpful comments on the manuscript and E. Burgh for a useful graphics routine. We acknowledge use of the Simbad Database at the Centre Données astronomiques de Strasbourg (<http://simbad.u-strasbg.fr/Simbad>).

REFERENCES

Baguhl, M., Grun, E., Landgraf, M. 1996, SSRv, 78, 165
Bohlin, R.C., Savage, B.D., & Drake, J.F. 1978, ApJ, 224, 132

Breitschwerdt, D. 1998, LNP, 506, 5

Buscombe, W. 1962, MtSOM, 4, 1

Buscombe, W. 1969, MNRAS, 144, 31

Cowley, A., Cowley, C., Jaschek, M., & Jaschek, C. 1969, AJ, 74, 375

Crawford, I.A. 1991, A&A, 247, 183

Dame, T.M. & Thaddeus, P. 1994, ApJ, 436, L173

Dickey, J.M. & Lockman, F.J. 1990, ARA&A, 28, 215

Diplas, A. & Savage, B.D. 1994, ApJ, 427, 274

Dring, A.R. 1997, PhD Thesis, The Johns Hopkins University

Dunkin, S.K. & Crawford, I.A. 1999, MNRAS, 302, 197

ESA 1997, The Hipparcos Catalogue, EAS SP-1200

Evans, D.S. 1967, Obs, 87, 286

Ferlet, R., Vidal-Madjar, A., & Gry, C. 1985, ApJ, 298, 838

Fitzpatrick, E.L. & Spitzer, L. 1994, ApJ, 427, 232

Frail, D.A., Weisberg, J.M., Cordes, J.M., & Mathers, C. 1994, ApJ, 436, 144

Frisch, P.C., Sembach, K., & York, D.G. 1990, ApJ, 364, 540

Ge'nova, R., Beckman, J.E., Bowyer, S., & Spicer, T. 1997, ApJ, 484, 761

Gordon, M.A. 1974, in *Methods of Experimental Physics*, Volume 12, edited by M.L. Meeks (Academic Press: New York), Chap. 6.1

Hiltner, W.A., Garrison, R.F., & Schild, R.E. 1969, ApJ, 157, 313

Hobbs, L.M. 1974a, ApJ, 188, L107

Hobbs, L.M. 1974b, ApJ, 191, 395

Hobbs, L.M. 1976, ApJ, 203, 143

Hoffleit, D. & Jaschek, C. 1982, The Bright Star Catalogue, New Haven, Conn., Yale University Observatory, 4th rev.ed.

Houk, N. 1982, Michigan Spectral Survey, Ann Arbor, Dept. of Astronomy, Univ. Michigan, Vol. 3

Houk, N. & Cowley, A. 1975, Michigan Spectral Survey, Ann Arbor, Dept. of Astronomy, Univ. Michigan, Vol. 1

Houk, N. & Smith-Moore, M. 1988, Michigan Spectral Survey, Ann Arbor, Dept. of Astronomy, Univ. Michigan, Vol. 4

Lallement, R. 1998, LNP, 506, 19L

Lallement, R. & Bertin, P. 1992, A&A, 266, 479

Lallement, R. & Ferlet, R. 1997, A&A, 324, 1105

Lauroesch, J.T., Meyer, D.M., & Blades, J.C. 1999, AAS, 72, 4

Lauroesch, J.T., Meyer, D.M., & Watson, J.K. 1998, ApJ, 507, L89

Levato, O.H. 1972, PASP, 84, 584

Linsky, J.L. & Wood, B.E. 1996, ApJ, 463, 254

Linsky, J.L., Redfield, S., Wood, B.E., & Piskunov, N. 2000, ApJ, in press

Martin, E.R. & York, D.G. 1982, ApJ, 257, 135

Murphy, D.C. & May, J. 1991, A&A, 247, 202

Pasquini, L., Duerbeck, H.W., Deiries, S., D'Odorico, S., & Reiss, R. 1992, Messenger, 69, 68

Redfield, S. & Linsky, J.L. 1999, ApJ, submitted

Sahu, M.S. 1992, Ph.D. Thesis, University of Groningen

Sfeir, D.M., Lallement, R., Crifo, F., & Welsh, B.Y. 1999, A&A, 346, 785

Snowden, S.L., Cox, D.P., McCammon, D., Sanders, W.T. 1990, ApJ, 354, 211

Spitzer, L. 1978, Physical Processes in the Interstellar Medium (New York: John Wiley)

Srinivasan Sahu, M. & Blaauw, A. 1994, Messenger, 76, 48

Stokes, G.M. 1978, ApJS, 36, 115

Toscano, M. *et al.* 1999, ApJ, 523, 171L

Vallerga, J.V., Vedder, P.W., & Welsh, B.Y. 1993, ApJ, 414, L65

Wallerstein, G., Silk, J., & Jenkins, E.B. 1980, ApJ, 240, 834

Watson, J.K. & Meyer, D.M., 1996, ApJ, 473, L127

Welsh, B.Y. 1991, ApJ, 373, 556

Welsh, B.Y., Craig, N., Vedder, P.W., & Vallerga, J.V. 1994, ApJ, 437, 638

Welsh, B.Y., Crifo, F., & Lallement, R. 1998, A&A, 333, 101

Welsh, B.Y., Vedder, P.W., & Vallerga, J.V. 1990, ApJ, 358, 473

Welty, D.E., Hobbs, L.M., & Kulkarni, V.P. 1994, ApJ, 436, 152

Willmarth, D. 1987, A CCD Atlas of Comparison Spectra: Thorium-Argon Hollow Cathode 3180–9540Å, Kitt Peak National Observatory

Wilson, R.E. 1953, General Catalogue of Stellar Radial Velocities (Washington D.C.: Carnegie Institutions)

Witte, M. *et al.* 1992, A&AS, 92, 333

York, D.G. 1983, ApJ, 264, 172

Figure Captions

Figure 1. A schematic diagram of the structures immediately surrounding the Sun. The Sun (at center) is embedded in the LIC and near the G cloud, which are both within the Local Bubble. Approximate locations, sizes, and angles subtended by the clouds are given by Linsky *et al.* (1999) and Lallement (1998). The velocities of the LIC and G cloud shown are with respect to the heliocentric frame of reference. The arrow extending from the Sun shows the direction of the motion of the Sun relative to the Local Standard of Rest (LSR). Dashed lines indicate the approximate angle subtended by Puppis-Vela.

Figure 2. Na I D₂ and D₁ spectra of 11 sight lines towards Puppis-Vela with $d < 200$ pc. Normalized intensity is plotted versus heliocentric velocity (km s^{-1}) for each star. The best-fit models to the absorption line profiles are shown as solid lines and the individual component fits are indicated by dashed lines. The bottom panel for each line of sight shows the residuals to the fits with the y-axis ranging from -0.1 to $+0.1$ for HD 72232 and HD 79416, and the y-axis ranging from -0.015 to $+0.015$ for all other lines of sight. The arrow on each plot indicates the projected LIC velocity for the particular sight line. †The complete Na I spectra toward HD 62226 and HD 74146 are shown in Figure 6.

Figure 3. Panel (a) shows the Galactic positions of the LISM stars towards the Puppis-Vela for which Na I spectra were obtained (filled symbols) and those for which Na I kinematic data was found in the literature (open symbols). Only stars at Galactic latitudes of $-10^\circ < b < +5^\circ$ have been included. Panel (b) shows where Na I was detected with velocities of $+6$ to $+9 \text{ km s}^{-1}$, (c) shows where velocities of $+12$ to $+15 \text{ km s}^{-1}$ were seen, and (d) gives the locations of $+21$ to $+23 \text{ km s}^{-1}$ Na I gas. In panels (b)-(d), the relative symbol size indicates the Na I column density. Small symbol: $10.00 \leq \log N(\text{Na I}) < 10.50$. Medium symbol: $10.50 \leq \log N(\text{Na I}) \leq 11.10$. Large symbol: $11.70 \leq \log N(\text{Na I}) \leq 12.60$.

Figure 4. The LISM stars in Puppis-Vela for which there exists Na I kinematic data, projected onto the Galactic plane. The distance to the stars increases radially, and the Galactic longitude increases along the arc. All stars have Galactic latitudes of $-10^\circ \leq b \leq +5^\circ$. The diamonds denote the sight lines in which (A) $+6 \leq V_{\text{helio}} \leq +9 \text{ km s}^{-1}$ Na I gas was detected, the triangles and squares mark where velocities of (B) $+12 \leq V_{\text{helio}} \leq +15 \text{ km s}^{-1}$ and (C) $+21 \leq V_{\text{helio}} \leq 23 \text{ km s}^{-1}$ Na I gas, respectively, were seen. The symbol sizes depict $N(\text{Na I})$ as defined for Figure 3. The arcs are drawn to indicate the maximum distance, and minimum extent in Galactic longitude of gas pockets with velocities A, B, and C. The stars shown are: 1) HD 103079, 2) HD 106490, 3) HD 93030, 4) HD 76805, 5) HD 74146, 6) HD 74071, 7) HD 74560, 8) HD 81188, 9) HD 79416, 10) HD 72232, 11) HD 61878, 12) HD 62226, 13) HD 64503.

Figure 5. Na I D₂ (top) and D₁ (middle) spectra along the line of sight to γ^2 Vel (HD 68273). The data points from each spectrum are represented as dots, a solid line indicates the best-fit model, and the dashed lines show the three components that compose the fit. The residual to the D₂ line fit is plotted at the bottom of the panel where the y-axis ranges between ± 0.05 .

Figure 6. Complete spectra for the eight lines to a) HD 62226 and b) HD 74146. In each panel, normalized intensity of the Na I D₂ lines are on top and D₁ lines are in the middle. At the bottom of each panel the residual to the D₂ model fits are shown with the y-axes ranging from -0.015 to $+0.015$. An IUE spectrum of HD 62226 was analyzed to help determine the origin of the high velocity components, but was inconclusive due to the low signal-to-noise ratio.

Figure 7. Na I absorption line data in the direction of the β CMa tunnel. The solid lines confine the first 200 pc of the β CMa tunnel as proposed by Welsh (1991) and the dotted lines outline the first 200 pc of the tunnel described in Welsh *et al.* (1998). The thick arc highlights the longitudinal extent of the β CMa tunnel according to the compilation of the data and pertains to the region below the Galactic plane where $-30^\circ < b < -10^\circ$. The arrows indicate that it is a lower limit on the distance to the end of the tunnel. Symbol sizes indicate the column density of Na I observed for given lines of sight as defined for Figure 3. If only an upper limit on the column density for a sight line is known, a downward triangle is used for the data point rather than a diamond. Filled symbols correspond to stars with $-10^\circ < b < 0^\circ$, and open symbols are used for stars with $-30^\circ < b < -10^\circ$.

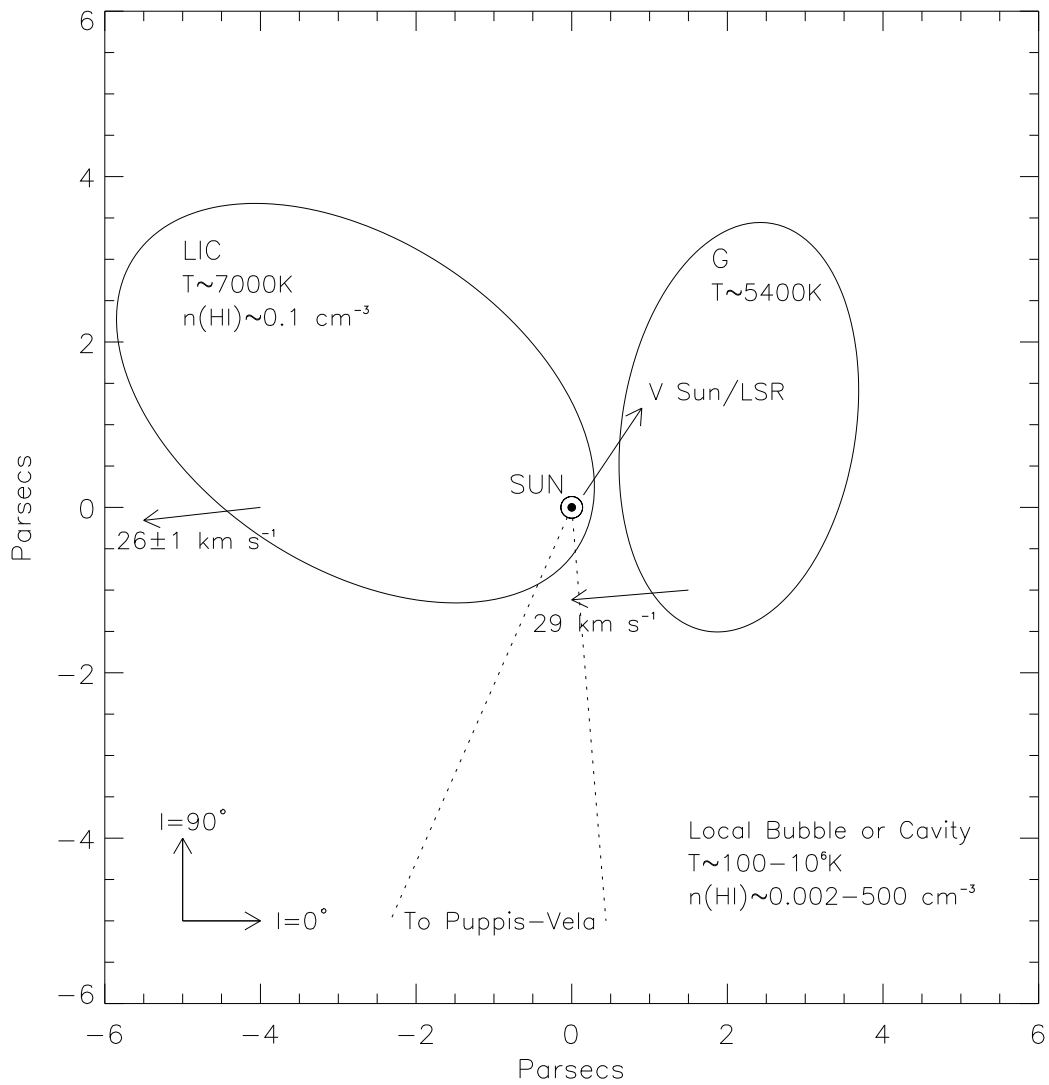


Figure 1

Table 1. Stellar Information—Targets Observed at ESO 1993-4

Object	l (°)	b (°)	MK	V ^a (mag)	B-V ^a (mag)	E _{B-V} ^b (mag)	d _{tp} ^c (pc)	v _{rad} (km s ⁻¹)	v sin i ^d (km s ⁻¹)	Refs. ^{e,f}
HD 61831	252.14	-7.90	B2.5 V	4.84	-0.173±.003	0.05	176±14	+26	138	2,6
HD 61878	252.01	-7.77	B5 V	5.76	-0.125±.004	0.05	188±18	+30	...	3,6
HD 62226	252.51	-7.70	B5 V	5.41	-0.133±.003	0.04	189±18	+40	100	4,6
HD 64503	253.90	-5.93	B2.5 V	4.49	-0.173±.004	0.05	196±20	-31	187	2,5
HD 65575	266.68	-12.32	B3 IVp	3.46	-0.162±.002	0.04	119±7	+19	95	2,5
HD 72232	263.91	-4.26	B7 IV	5.98	-0.129±.004	-0.01	193±20	+12	...	1,5
HD 74071	270.59	-7.22	B5 V	5.45	-0.135±.004	0.04	138±9	+15	128	2,5
HD 74146	270.33	-6.92	B4 IV	5.18	-0.129±.004	0.06	131±8	+14	56	2,5
HD 74560	270.60	-6.66	B3 V	4.83	-0.159±.004	0.04	147±10	+22	22	2,5
HD 76805	271.62	-4.79	B5 V	4.71	-0.119±.004	0.05	115±7	+22	48	2,6
HD 79416	266.63	+3.30	...	5.98	-0.109±.006	...	191±25	+15	384	...,5

^aV and B-V values are from the Tycho Catalogue.

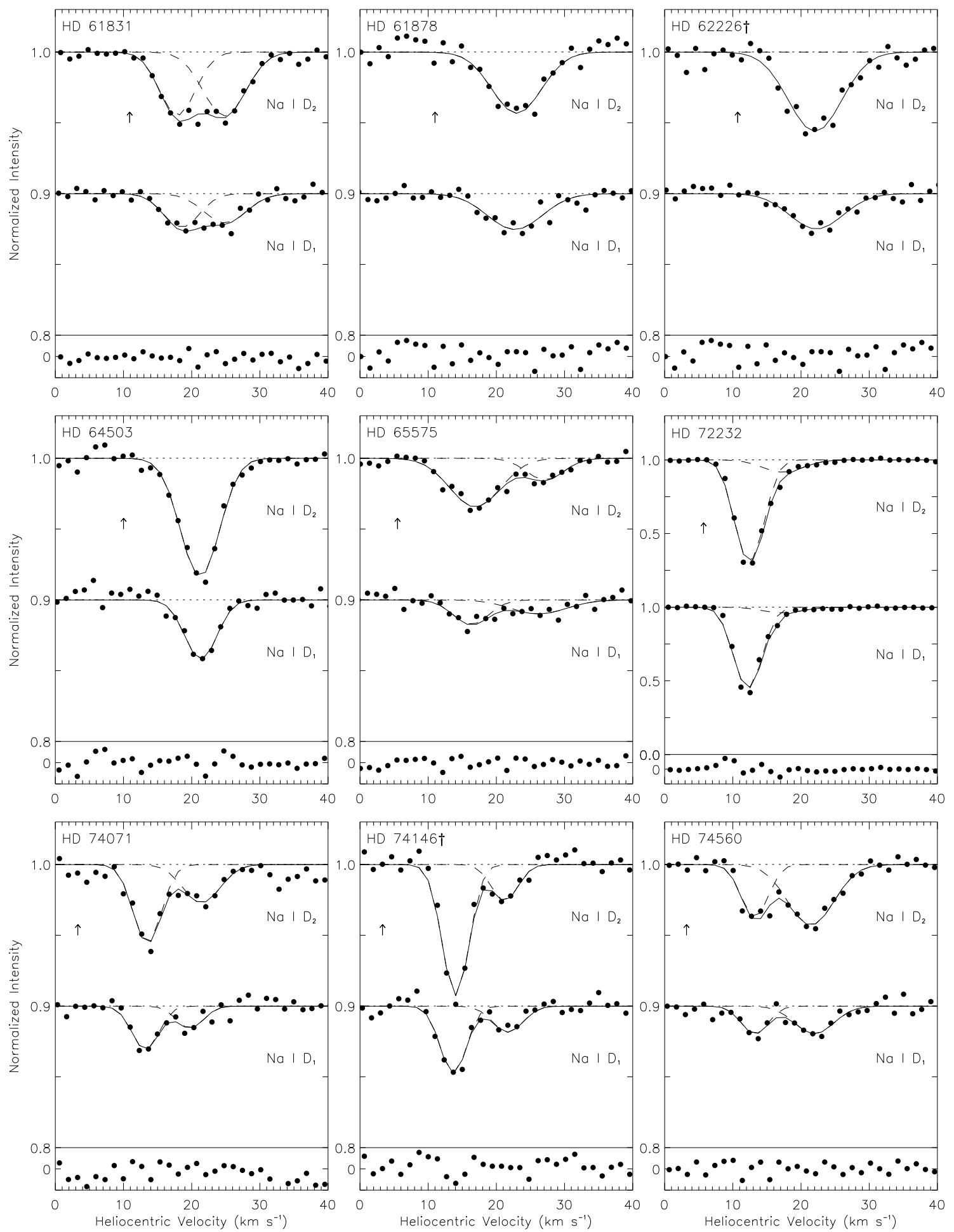
^bCalculated using (B-V) and MK type listed, and (B-V)₀ from Mihalas & Binney (1981)

^cDistance and error calculated from Hipparcos parallax data.

^dTaken from Hoffleit & Jaschek (1982).

^eMK References: (1)Buscombe 1969; (2) Hiltner, Garrison, & Schild 1969; (3) Houk 1982; (4) Houk & Cowley, 1975

^fV_{rad} References: (5) Evans 1967; (6) Wilson 1953



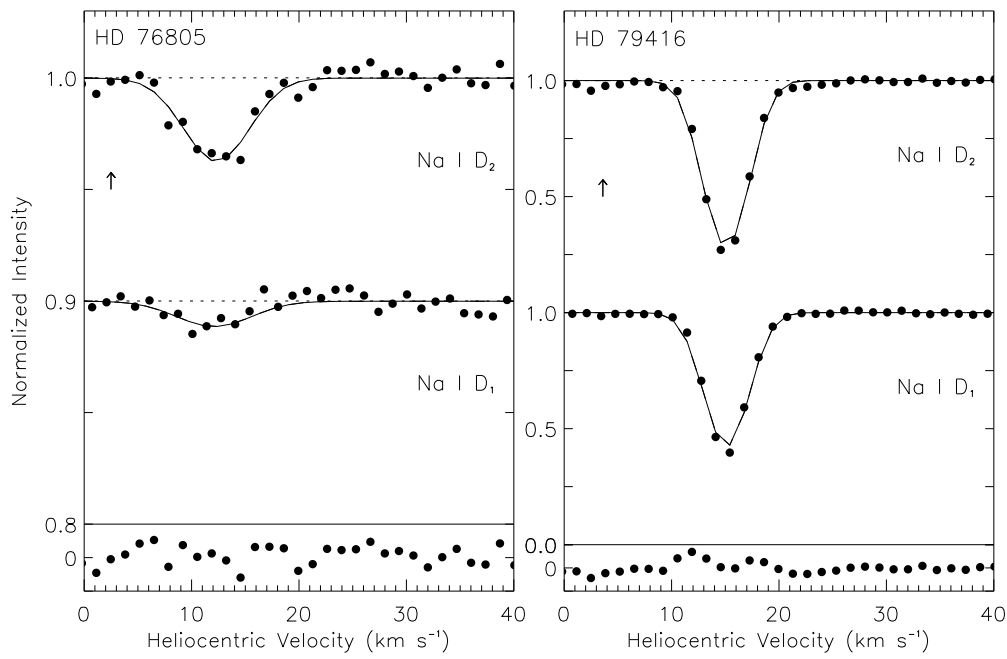


Figure 2

Table 2. Na I D Model Fit Parameters—Targets Observed at ESO 1993-4

Object	V_{helio}^a (km s^{-1})	$W_\lambda(D_2)^b$ (mÅ)	b^b (km s^{-1})	$\log N(\text{Na I})^{b,c}$ (cm^{-2})	S/N	ΔV^d (km s^{-1})
HD 61831	+18.2	5.8a	3.1a	10.49a	250	–14.95
	+24.9	6.9a	3.9a	10.54a		
HD 61878	+22.9	7.7a	5.0a	10.66a	165	–14.95
HD 62226	–10.6	<4	...	<10.10	170	–14.90
	+22.2	11a	5.1a	10.72a		
	+132.3	4.8a	5.3a	10.48a		
HD 64503	+21.3	12a	3.1b	10.75a	210	–14.62
HD 65575	+16.9	6.3a	4.5a	10.48a	240	–13.64
	+27.2	2.1a	3.3a	10.10a		
HD 72232	+12.3	76a	1.9a	11.86a	225	–13.31
	+17.3	13a	3.6a	10.79a		
HD 74071	+13.4	5.7a	2.0c	10.49a	160	–12.63
	+20.7	3.6a	2.6c	10.24a		
HD 74146	–139	16a	16.7a	11.13a	150	–12.64
	+13.9	8.2a	1.9b	10.69a		
	+21.4	2.8a	1.9b	10.16a		
HD 74560	+13.2	3.6a	1.9a	10.28a	200	–12.58
	+21.7	7.2a	3.9b	10.51a		
HD 76805	+12.2	6.1a	4.2a	10.40a	200	–12.23
HD 79416	+15.1	74a	1.9a	11.75a	110	–12.03

^aVelocity uncertainty is $\pm 0.5 \text{ km s}^{-1}$.

^b(a) error < 10%; (b) error 10 to 20%; (c) uncertain, D₁ line components are weak and blended

^cAverage column density of D₂ and D₁ lines.

^d $V_{LSR} = V_{helio} + \Delta V$.

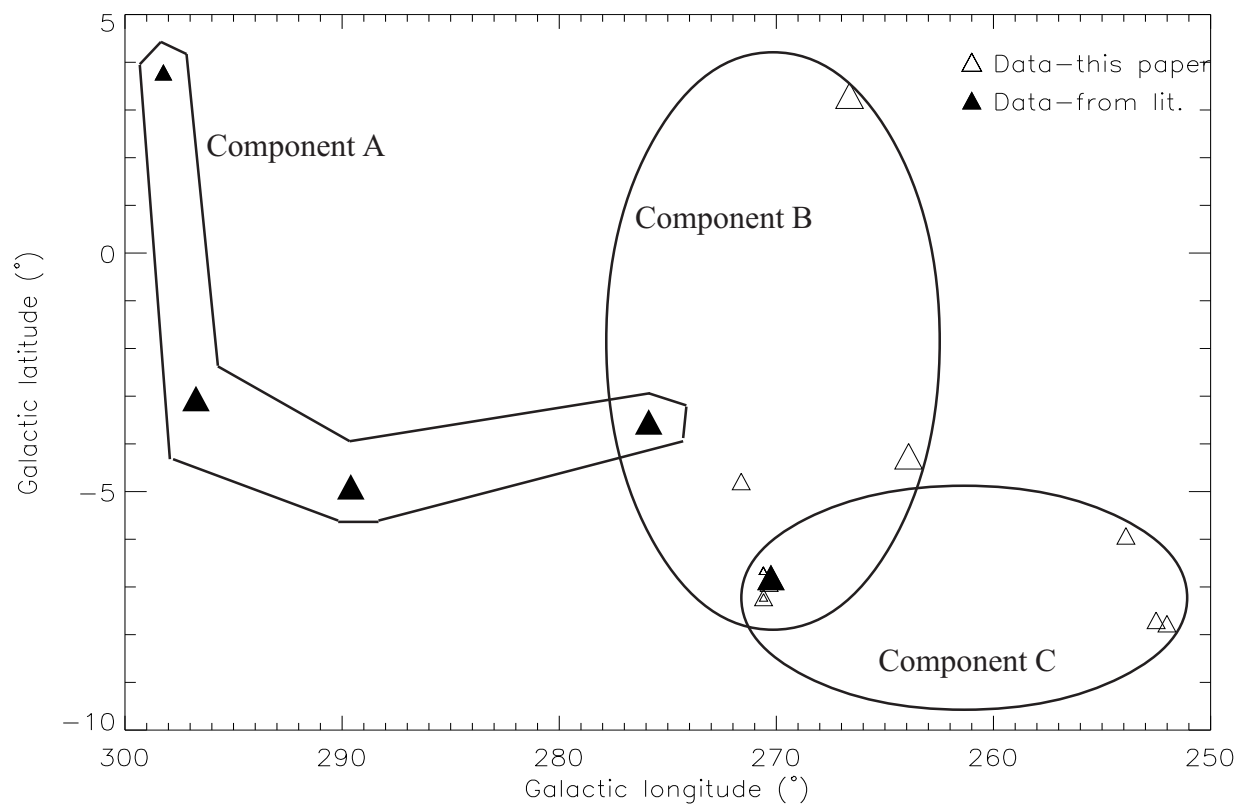


Figure 3

Table 3. Stellar Information for Published Sight Lines

Object	l ($^{\circ}$)	b ($^{\circ}$)	MK	V ^a (mag)	B-V ^a (mag)	E _{B-V} ^b (mag)	d _{tp} ^c (pc)	v _{rad} (km s $^{-1}$)	v sin i ^d (km s $^{-1}$)	Refs. ^{e,f}
HD 74195	270.25	-6.80	B3 IV	3.60	-0.159 \pm .003	0.04	152 \pm 12	+16	40	1,3
HD 81188	275.88	-3.54	B2 IV-V	2.48	-0.143 \pm .004	0.10	165 \pm 13	+22	49	1,3
HD 93030	289.60	-4.90	B0.5 Vp	2.74	-0.200 \pm .002	0.08	135 \pm 9	+24	151	1,3
HD 103079	296.73	-3.05	B4 V	4.94	-0.132 \pm .006	0.05	104 \pm 6	+21	57	2,3
HD 106490	298.23	+3.79	B2 IV	2.79	-0.194 \pm .002	0.05	112 \pm 7	+22	194	1,3

^aV and B-V values are from the Tycho Catalogue.

^bCalculated using (B-V) and MK type listed, and (B-V)₀ from Mihalas & Binney (1981)

^cDistance and error calculated from Hipparcos parallax data.

^dTaken from Hoffleit & Jaschek (1982).

^eMK References: (1) Hiltner, Garrison, & Schild 1969; (2) Simbad Database

^fV_{rad} Reference: (3) Evans 1967

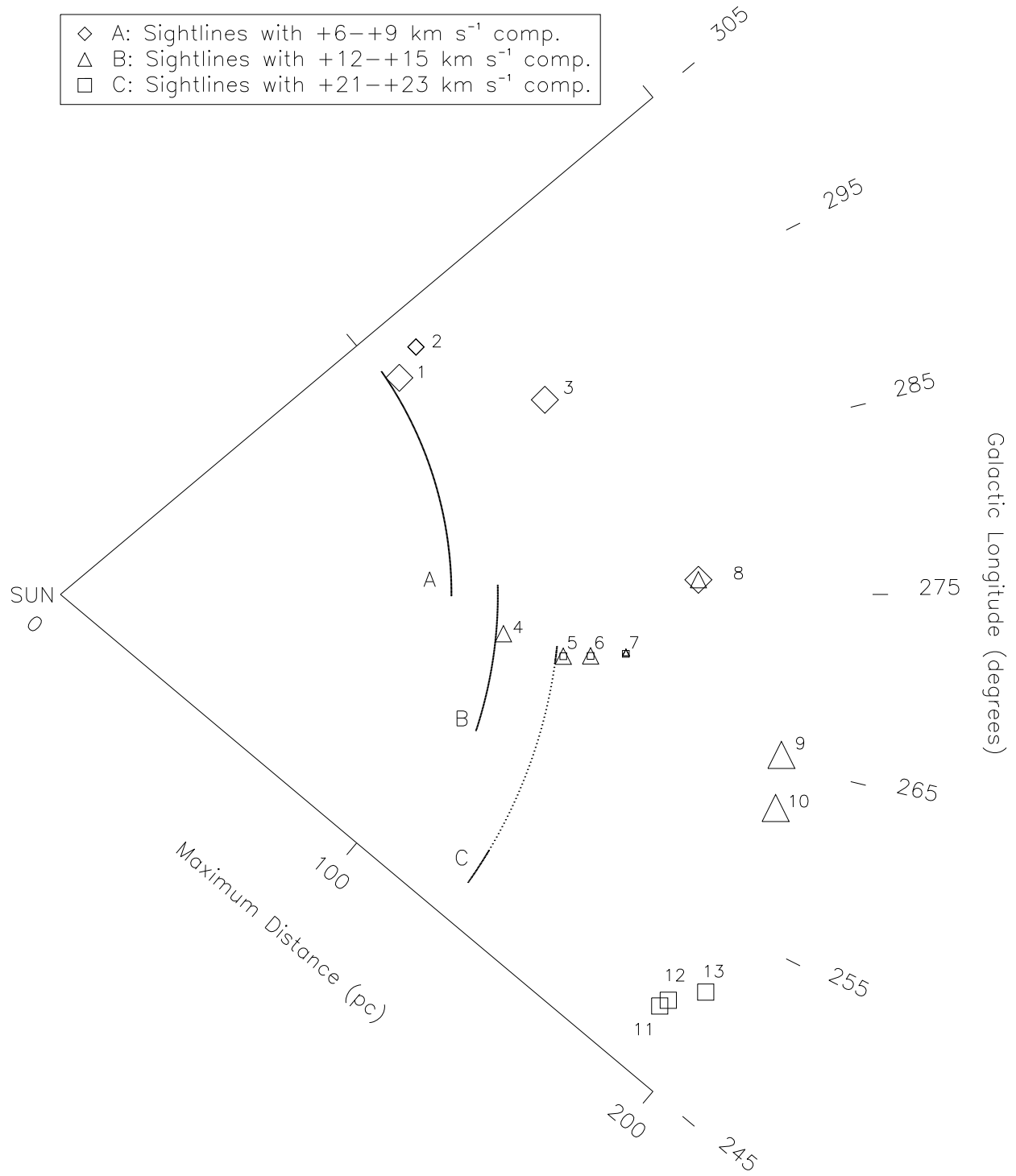


Figure 4

Table 4. Na I Spectroscopic Data for Published LISM Sight Lines

Object	V_{helio} (km s^{-1})	b (km s^{-1})	log N (cm^{-2})	Velocity Res. (km s^{-1})	Ref. ^a
HD 74195	+13.2	0.3 ± 0.1	10.98	3.6	4
HD 81188	+8.0	1.0	11.90	3.6	1
	$+8.3 \pm 0.1$	0.72 ± 0.09	11.74	0.32	2
	$+8.6 \pm 0.1$	0.46 ± 0.05	11.58	0.32	2
	+13.0	3.0	11.08	3.6	1
	$+12.1 \pm 0.1$	1.4 ± 0.1	11.07	0.32	2
	$+13.8 \pm 0.4$	1.4 ± 0.2	10.45	0.32	2
	$+16.6 \pm 0.3$	1.75 ± 0.3	10.45	0.32	2
HD 93030	+8.0	...	11.81	3	3
HD 103079	+8.3	5.0 ± 1.0	11.02	3.6	1
HD 106490	<9.85	3.6	1
	-0.4	1.0 ± 1.0	10.54	3.6	1
	+6.2	2.0 ± 1.0	10.48	3.6	1

^aReferences: (1) Crawford, 1991; (2) Dunkin & Crawford, 1999; (3) Ferlet, Vidal-Madjar, & Gry, 1985; (4) Welsh *et al.*, 1994

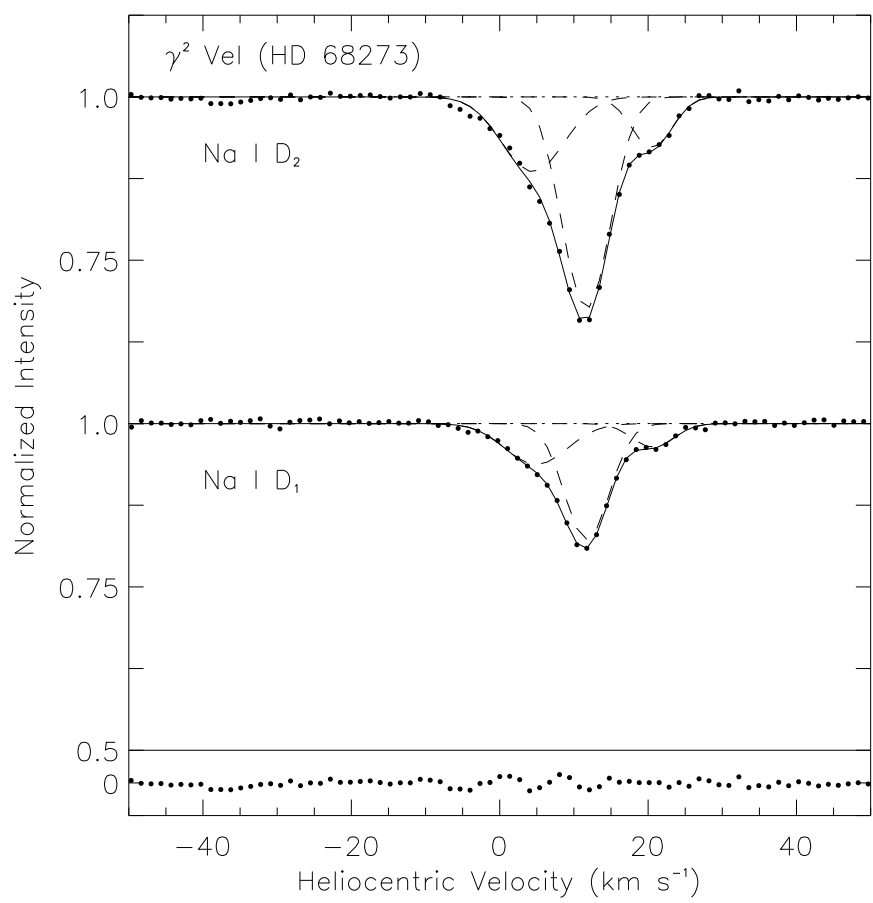


Figure 5

Table 5. Properties of Gas A, B, and C

Property	A	B	C
Galactic Longitude	275.9° to 298.2°	263.9° to 275.9°	252.0° to 270.6°
Galactic Latitude	-4.9° to $+3.8^\circ$	-7.2° to $+3.3^\circ$	-7.8° to -5.9°
Maximum Distance	~ 104 pc	~ 115 pc	~ 131 pc
Heliocentric Gas Velocity	$+6$ to $+9$ km s^{-1}	$+12$ to $+15$ km s^{-1}	$+21$ to $+23$ km s^{-1}
Range of $\log N(\text{Na I})$	10.5 to 11.8 cm^{-2}	10.3 to 11.9 cm^{-2}	10.2 to 10.8 cm^{-2}

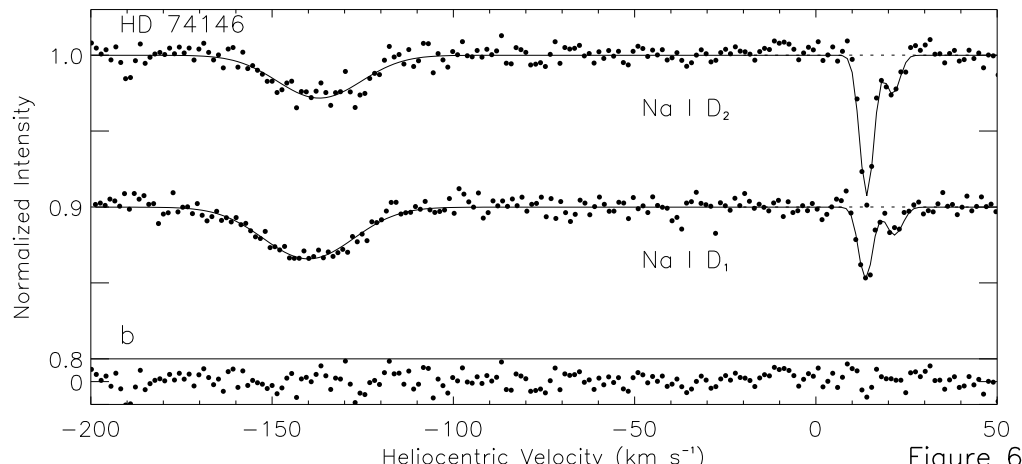
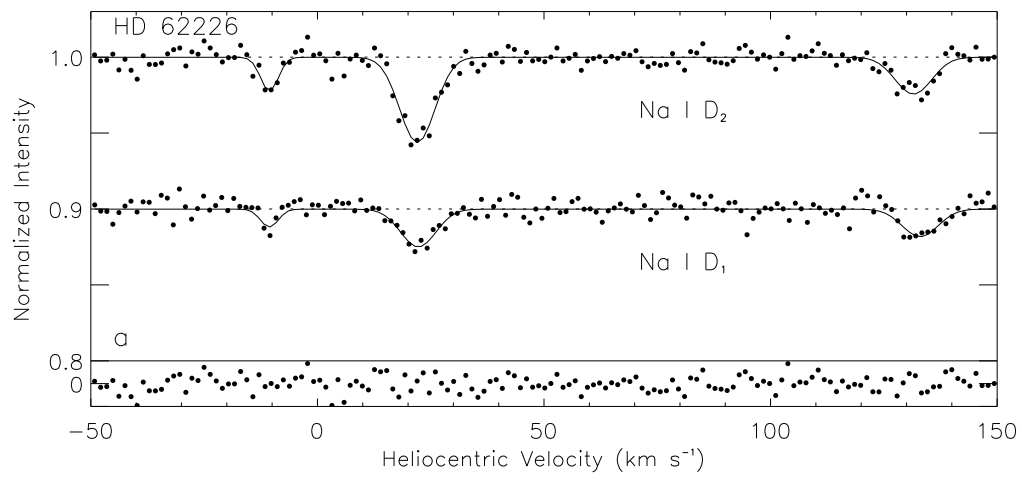


Figure 6

Table 6. Nomenclature of Interstellar Absorption Components toward γ^2 Vel

FS94 V_{helio} (km s^{-1})	Component Name FS94	Component Name This Paper
-5.1 ± 0.4	1	...
$+4.5 \pm 0.1$	2	...
$+5.2 \pm 0.2$	3	...
$+12.7 \pm 0.2$	4	B
$+15.4 \pm 0.9$	5	B
$+21.4 \pm 0.1$	6	C
$+26.7 \pm 0.2$	7	...

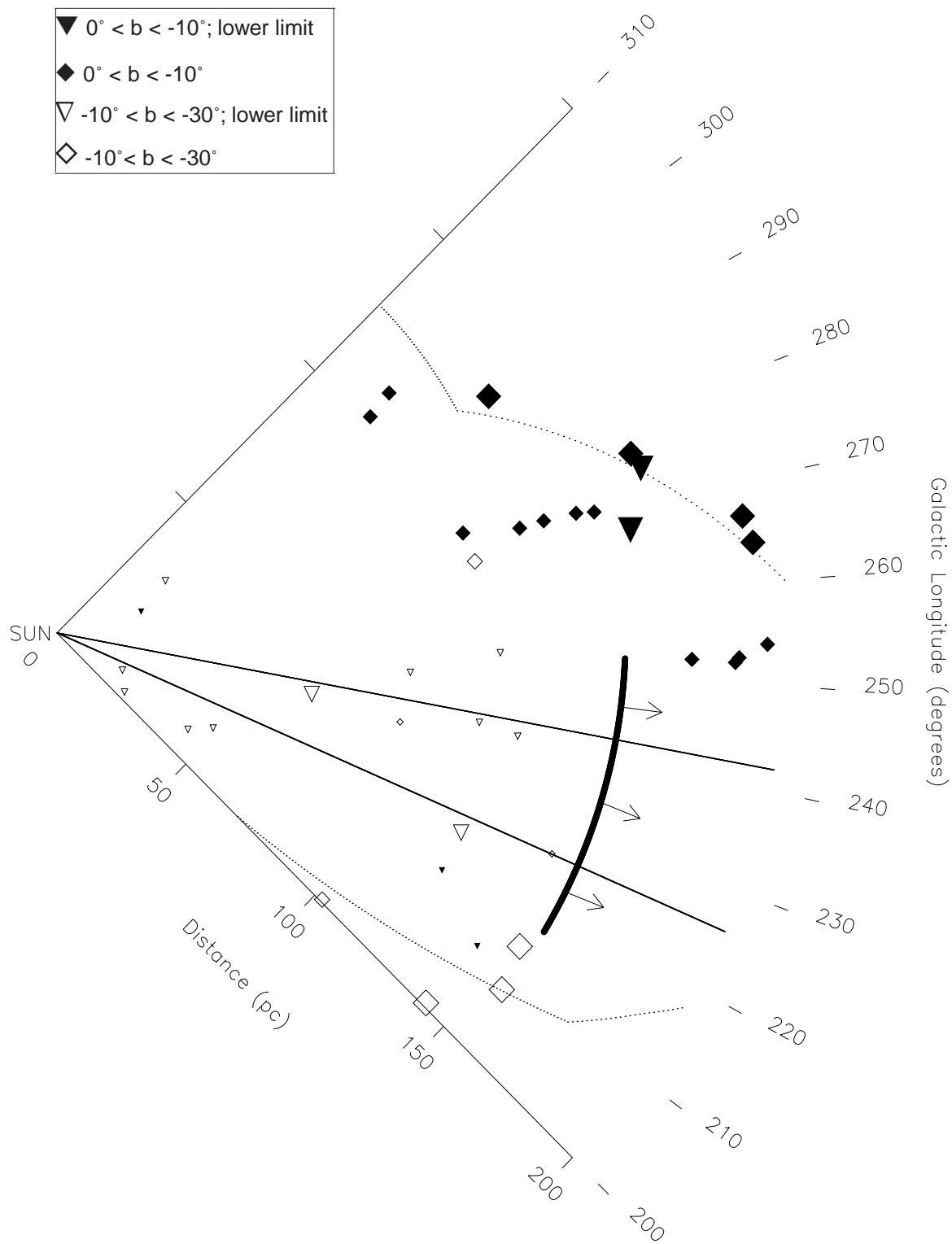


Table 7. γ^2 Vel Na I D Model Fit Parameters

V_{helio}^a (km s^{-1})	$W_{\lambda}(D_2)^b$ (mÅ)	b^b (km s^{-1})	$\log N(\text{Na I})^{b,c}$ (cm^{-2})	Component FS94	Component This Paper
+4.6	20	5.5	11.12	2	...
+11.7	55	3.8	11.48	4	B
+20.6	10	3.3	10.73	6	C

^aVelocity uncertainty is $\pm 0.5 \text{ km s}^{-1}$.

^bError $< 10\%$

^cAverage column density of D₂ and D₁ lines.

Table 8. Stellar Information—Additional Targets from Literature

Object	l ($^{\circ}$)	b ($^{\circ}$)	MK	V ^a (mag)	B-V ^a (mag)	E _{B-V} ^b (mag)	d _{tp} ^c (pc)	v _{rad} (km s $^{-1}$)	v sin i ^d (km s $^{-1}$)	Refs. ^{e,f}
HD 30211	200.53	-29.34	B5 IV	4.02	-0.133 \pm 0.004	0.03	163 \pm 27	+9	140	2,10
HD 33111	205.34	-25.32	A3 III	2.79	0.151 \pm 0.003	0.06	27 \pm 1	-9	179	8,10
HD 33904	217.25	-28.91	B9 IV:HG MN	3.29	-0.095 \pm 0.002	-0.04	57 \pm 2	+28	12	7,11
HD 33949	213.88	-27.55	B7 V	4.43	-0.098 \pm 0.006	0.02	172 \pm 20	+18	124	7,11
HD 34503	208.28	-23.96	B5 III	3.60	-0.110 \pm 0.002	0.05	170 \pm 22	+20	46	2,11
HD 34968	223.35	-29.07	A0 V	4.74	-0.047 \pm 0.002	-0.03	141 \pm 13	+30	51	7,11
HD 36777	200.43	-15.27	A2 V	5.33	0.055 \pm 0.003	-0.01	106 \pm 8	-4	145	3,10
HD 37507	211.16	-19.40	A4 V	4.79	0.139 \pm 0.003	0.02	47 \pm 5	-1	170	3,10
HD 37795	238.81	-28.86	B7 IV	2.66	-0.091 \pm 0.003	0.03	82 \pm 4	+35	176	5,11
HD 38678	219.40	-20.83	A2 Vann	3.55	0.113 \pm 0.003	0.05	22 \pm 1	+20	202	7,11
HD 42824	210.74	-9.75	A2 V	6.63	0.053 \pm 0.007	-0.01	145 \pm 16	3, ...
HD 44402	237.52	-19.43	B2.5 IV	3.02	-0.163 \pm 0.002	0.06	103 \pm 6	+32	63	4,10
HD 44743	226.06	-14.27	B1 II	1.96	-0.164 \pm 0.007	0.06	153 \pm 15	+34	36	1,11
HD 45380	216.86	-8.89	A0 Vn	6.33	-0.041 \pm 0.004	-0.02	125 \pm 18	...	146	9, ...
HD 45813	240.64	-18.76	B4 V	4.47	-0.156 \pm 0.002	0.03	125 \pm 9	+41	135	4,11
HD 47670	251.94	-20.54	B8 III	3.18	-0.098 \pm 0.003	-0.01	130 \pm 9	+28	228	1,11
HD 49591	247.37	-17.03	B8/B9 V	5.27	-0.081 \pm 0.003	0.02	102 \pm 6	+47	173	5,11
HD 52089	239.83	-11.33	B2 II	1.53	-0.132 \pm 0.007	0.07	132 \pm 10	+27	44	1,10
HD 74956	272.08	-7.37	A0 V	1.94	0.086 \pm 0.003	0.11	24 \pm 0.2	+2	40	6,11
HD 75311	273.90	-8.41	B3 Vne	4.50	-0.168 \pm 0.002	0.03	168 \pm 12	+27	332	4,11
HD 79694	267.21	+3.14	B6 IV	5.85	-0.115 \pm 0.004	0.03	160 \pm 14	+22	260	4,10
HD 80007	285.98	-14.41	A0 III	1.67	0.060 \pm 0.007	0.06	34 \pm 5	-5	133	1,11

^aV and B-V values are from the Tycho Catalogue.

^bCalculated using (B-V) and MK type listed, and (B-V)₀ from Mihalas & Binney (1981)

^cDistance and error calculated from Hipparcos parallax data.

^dTaken from Hoffleit & Jaschek (1982).

^eMK References: (1) Buscombe 1962; (2) Buscombe 1969; (3) Cowley *et al.* 1969; (4) Hiltner, Garrison, & Schild 1969; (5) Houk 1982; (6) Houk & Cowley, 1975; (7) Houk & Smith-Moore, 1988; (8) Levato, 1972; (9) Simbad Database

^fV_{rad} References: (10) Evans 1967; (11) Wilson 1953

Table 9. Na I Spectroscopic Data for LISM Sight Lines—Additional Targets from Literature

Object	log N (cm ⁻²)	Ref. ^a
HD 30211	12.11	8 ^b
HD 33111	<10.25	8 ^b
HD 33904	<10.04	7 ^b
HD 33949	10.60	8 ^b
	11.71	8 ^b
HD 34503	11.41	2 ^b
HD 34968	<10.37	8 ^b
HD 36777	10.4	3
HD 37507	<10.00	2 ^b
HD 37795	<10.36	7 ^b
HD 38678	<10.23	7 ^b
HD 42824	<10.3	3
HD 44402	10.20	7 ^b
HD 44743	10.00	1
	10.00	6
	<10.00	4
HD 45380	<10.3	3
HD 45813	<10.11	8
HD 47670	<10.23	8
HD 49591	<10.28	8
HD 52089 a	<10.20	7
HD 65575	<10.20	8
HD 74956	<10.11	8
HD 75311	<11.51	5
HD 79694	<11.80	5
HD 80007	<10.23	8

^aReferences: (1) Ferlet, Vidal-Madjar, & Gry, 1985; (2) Frisch, Sembach, & York, 1990; (3) Sfeir *et al.*, 1999; (4) Vallerga, Vedder, & Welsh, 1993; (5) Wallerstein, Silk, & Jenkins, 1980; (6) Welsh, Vedder, & Vallerga, 1990; (7) Welsh, 1991; (8) Welsh *et al.*, 1994

^bData compiled by Dring (1997), in Table 5.1